

A HARD IONIZING SPECTRUM IN $Z = 3 - 4$ $\text{Ly}\alpha$ EMITTERS WITH INTENSE $[\text{O III}]\lambda 5007$ EMISSION: ANALOGS OF GALAXIES IN THE REIONIZATION ERA? ^{† ‡}

KIMIIHIKO NAKAJIMA^{1,2}, RICHARD S. ELLIS^{1,3}, IKURU IWATA⁴, AKIO K. INOUE⁵, HARUKA KUSAKABE⁶, MASAMI OUCHI^{7,8},
 AND BRANT E. ROBERTSON⁹

submitted to ApJ Letters on Aug 27, 2016

ABSTRACT

We present Keck/MOSFIRE spectra of the diagnostic nebular emission lines $[\text{O III}]\lambda\lambda 5007, 4959$, $[\text{O II}]\lambda 3727$, and $\text{H}\beta$ for a sample of 15 redshift $z \simeq 3.1 - 3.7$ $\text{Ly}\alpha$ emitters (LAEs) and Lyman break galaxies (LBGs). In conjunction with spectra from other surveys, we confirm earlier indications that LAEs have a much higher $[\text{O III}]/[\text{O II}]$ line ratio than is seen in similar redshift LBGs. By comparing their distributions on a $[\text{O III}]/[\text{O II}]$ versus R23 diagram, we demonstrate that this difference cannot arise solely because of their lower metallicities but most likely is due to a harder ionizing spectrum. Using measures of $\text{H}\beta$ and recombination theory, we demonstrate, for a subset of our LAEs, that ξ_{ion} - the number of Lyman continuum photons per UV luminosity - is indeed $0.2 - 0.5$ dex larger than for typical LBGs at similar redshifts. Using photoionization models we estimate the effect this would have on both $[\text{O III}]/[\text{O II}]$ and R23 and conclude such a hard spectrum can only partially explain such intense line emission. The additional possibility is that such a large $[\text{O III}]/[\text{O II}]$ ratio is in part due to density rather than ionization bound nebular regions, which would imply a high escape fraction of ionizing photons. We discuss how further observations could confirm this possibility. Clearly LAEs with intense $[\text{O III}]$ emission represent a promising analog of those $z > 7$ sources with similarly strong lines which are thought to be an important contributor to cosmic reionization.

Subject headings: galaxies: evolution — galaxies: high-redshift.

1. INTRODUCTION

To understand how cosmic reionization occurred during the redshift range $6 < z < 10$, it is necessary to identify the responsible sources. Due to the steep decrease of the number density of quasars with redshift at $z > 3$ (Fan et al. 2004), the currently popular viewpoint is that star-forming galaxies played the dominant role in

delivering the necessary ionizing photons into the intergalactic medium (IGM; Robertson et al. 2015).

The key question is whether the typical output of ionizing photons from $6 < z < 10$ galaxies is sufficient. This requires knowledge of (i) the UV radiation emerging from their stellar populations, defined by Robertson et al. (2013) in terms of ξ_{ion} , the number of Lyman continuum (LyC) photons per $\text{UV}(1500 \text{ \AA})$ luminosity and (ii) the fraction f_{esc} of such LyC photons that can escape scattering within the galaxy and its immediate vicinity. Neither of these important quantities is currently constrained for early galaxies so this is the primary uncertainty in claims that reionization is driven primarily by star-forming galaxies.

The present Letter is motivated by finding observational evidence that the ionizing spectrum is harder, and that ξ_{ion} and f_{esc} both increase with redshift, particularly for low mass, metal-poor systems characteristic of those that likely dominate reionization. Intense nebular emission, e.g., of $[\text{O III}]\lambda 5007$, appears to be more common in high redshift galaxies (Schenker et al. 2013; Smit et al. 2014, 2015) and this has been interpreted as evidence for a harder ionizing spectrum. Although such emission lines are not directly accessible with ground-based spectrographs beyond $z \sim 5$, IRAC photometry can still trace their presence via an excess inferred in the SEDs. The most intense $[\text{O III}]$ emitters at $z > 7$ located via IRAC photometry have confirmed $\text{Ly}\alpha$ emission (Zitrin et al. 2015; Roberts-Borsani et al. 2015) which suggests they may have already created significant ionized bubbles for which a high value of f_{esc} is necessary (Stark et al. 2016).

Since neither ξ_{ion} nor f_{esc} cannot directly be observed beyond $z \simeq 6$, we seek to find and study analogs of the reionization sources at $z \simeq 3$, the highest redshift

knakajim@eso.org

¹ European Southern Observatory, Karl-Schwarzschild-Str. 2, 85748, Garching bei Munchen, Germany

² Observatoire de Genève, Université de Genève, 51 Ch. des Maillettes, 1290 Versoix, Switzerland

³ Department of Physics and Astronomy, University College London, Gower Street, London, WC1E 6BT, UK

⁴ Subaru Telescope, National Astronomical Observatory of Japan, 650 North A'ohoku Place, Hilo, HI 96720, USA

⁵ College of General Education, Osaka Sangyo University, 3-1-1 Nakagaito, Daito, Osaka 574-8530, Japan

⁶ Department of Astronomy, Graduate School of Science, The University of Tokyo, 7-3-1 Hongo, Bunkyo-ku, Tokyo 113-0033, Japan

⁷ Institute for Cosmic Ray Research, The University of Tokyo, 5-1-5 Kashiwanoha, Kashiwa, Chiba 277-8582, Japan

⁸ Kavli Institute for the Physics and Mathematics of the Universe (WPI), The University of Tokyo, 5-1-5 Kashiwanoha, Kashiwa, Chiba 277-8583, Japan

⁹ Department of Astronomy and Astrophysics, University of California, Santa Cruz, 1156 High Street Santa Cruz, CA 95064, USA

[†] Some of the data presented herein were obtained at the W.M. Keck Observatory, which is operated as a scientific partnership among the California Institute of Technology, the University of California and the National Aeronautics and Space Administration. The Observatory was made possible by the generous financial support of the W.M. Keck Foundation.

[‡] The observations were carried out within the framework of Subaru-Keck time exchange program, where the travel expense was supported by the Subaru Telescope, which is operated by the National Astronomical Observatory of Japan.

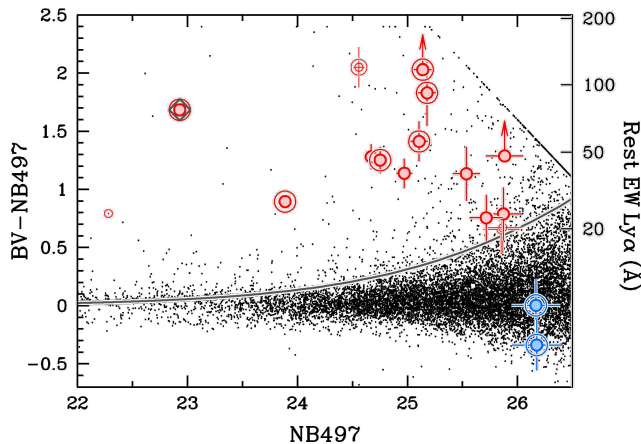


FIG. 1.— Color-magnitude diagram of BV-NB497 vs. NB497 for the SSA22 field (where BV refers to $(2B+V)/3$). Black dots show all the photometric detections. The grey curve presents the 4σ photometric error in BV-NB497. Large circles with error-bars show candidate $z \simeq 3.1$ LAEs (red), LBGs (blue) and AGN-LAE (red with a grey diamond) observed with MOSFIRE. Filled and open circles present LAEs and LBGs confirmed and unconfirmed respectively with MOSFIRE. Objects with prior optical spectroscopic confirmation are marked with a second circle.

where direct measures of these quantities are possible. The inter-dependence of strong [O III] emission and the leakage of LyC photons was first evaluated in the context of photoionization models by Nakajima & Ouchi (2014). They suggested that large values of the emission line ratio $[\text{O III}]\lambda 5007/[\text{O II}]\lambda 3727$ may indicate a high value of f_{esc} . Furthermore, the $[\text{O III}]/[\text{O II}]$ ratio is sensitive to the ionization parameter q_{ion} , which is, in ionization equilibrium, related to the ionizing photon production rate Q_{H^0} , such that

$$q_{\text{ion}} \propto (Q_{\text{H}^0} \times n_{\text{H}})^{1/3}, \quad (1)$$

where n_{H} is the gas density. A correlation between $[\text{O III}]/[\text{O II}]$ ratio and ξ_{ion} is thus suggested. Recent support for these conjectures are provided by significant LyC radiation detected in nearby intense [O III] emitters (Izotov et al. 2016a,b; Schaerer et al. 2016).

In this Letter, we use the Keck near-infrared spectrograph MOSFIRE to compare the physical properties of a representative sample of intense [O III]-emitting Lyman alpha emitters (LAEs) at $z \simeq 3$ with equivalent data for Lyman break galaxies (LBGs). Our goal is to understand their $[\text{O III}]/[\text{O II}]$ line ratios in terms of a hard ionizing spectrum. Ultimately we seek to verify that such sources may also have a high f_{esc} and thus represent valuable analogs of the star-forming galaxies responsible for cosmic reionization.

2. SPECTROSCOPIC DATA

2.1. Sample

Our target sample is drawn from a Subaru imaging survey which has identified $z \simeq 3.1$ LAEs in the SSA22 field (Hayashino et al. 2004; Yamada et al. 2012; Micheva et al. 2015). LAEs at $z \simeq 3.1$ were selected via their photometric excess in a narrow band filter centered at 497nm (Figure 1). A limited amount of confirmatory optical spectroscopy has already been conducted for this sample.

For the present campaign, we selected 16 LAEs from this sample which lie within an appropriately placed

MOSFIRE 4×6 arcmin field. We also included 2 $z \simeq 3.1$ LBGs and one $z \simeq 3.7$ LAE. The $z \simeq 3.7$ LAE was initially classed as a LBG but optical spectroscopy revealed strong Ly α emission. Among the total of 19 targets, 10 were already confirmed from previous optical spectroscopy. One of the $z = 3.1$ LAEs is a Type II AGN (Micheva et al. 2016) but the other targets show no obvious indications of AGN activity.

2.2. Observation and Data reduction

Observations were undertaken on UT 2015 June 20 and 21. Both nights were photometric with a seeing of $0''.45$ – $0''.50$. MOSFIRE multi-slit spectroscopy was taken using the H and K band filters sampling the wavelength ranges of 1.45 – 1.78 and 1.92 – $2.37 \mu\text{m}$, respectively. Using a slit width of $0''.7$ the resolving power is $R \sim 3700$ in the H band and 3600 in K . Individual exposures of 180 sec (120 sec) were taken in K (H) with a AB nod sequence of $3''.0$ separation. The total integration time was 2.5 hours in H and 3.0 hours in K .

Data reduction was performed using the MOSFIRE DRP¹². The processing includes flat fielding, wavelength calibration, background subtraction and combining the nod positions. Wavelength solutions in H were obtained from OH sky lines, while in K a combination of OH lines and Ne arcs was used.

Flux solutions and telluric absorption corrections were obtained from A0V *Hipparcos* stars observed at similar airmasses. This procedure also corrects for slit-losses since LAEs are unresolved in typical ground-based conditions (Malhotra et al. 2012) and the standard stars were observed in a similar manner. Flux calibrations were independently confirmed using a relatively bright star ($K_{\text{Vega}} = 16.2$) placed on the mask.

2.3. Emission line identifications

One or more emission lines were detected at the $> 3\sigma$ level in 17 of our 19 targets. Based on previously spectroscopic redshifts and the expected redshift of $z \simeq 3.1$ for the bulk of the sample, 15 sources (12 LAEs and two LBGs at $z \simeq 3.1$ and one LAE at $z \simeq 3.7$) are readily identified with $[\text{O III}]\lambda 5007$. Two are considered to be H α at $z \sim 1.6$ and two further faint targets present no significant signal. The following analysis is therefore based on the successfully confirmed 15 sources.

We measured $[\text{O II}]$ ¹³, $[\text{O III}]$ and H β line fluxes by fitting a Gaussian profile to each line with the IRAF task `specfit` in `stdas.contrib.specfitpkg`. In the fitting procedure, the redshift and FWHM of the $[\text{O III}]\lambda 5007$ (i.e., the strongest emission line) were adopted as Gaussians for the other lines. An H+K spectrum of a representative $z \simeq 3.1$ LAE with a demonstrating of the fitting process is shown in Figure 2.

Table 1 lists the measured $[\text{O III}]/[\text{O II}]$ ratio and the R23-index, $([\text{O III}]\lambda\lambda 5007, 4959 + [\text{O II}]\lambda 3727)/\text{H}\beta$, for each of the 15 targets.

3. RESULTS

3.1. The $[\text{O III}]/[\text{O II}]$ ratio of LAEs and LBGs

¹² <https://keck-datareductionpipelines.github.io/MosfireDRP>. See also Steidel et al. (2014).

¹³ We use the notation $[\text{O II}]\lambda 3727$ as the sum of the doublet.

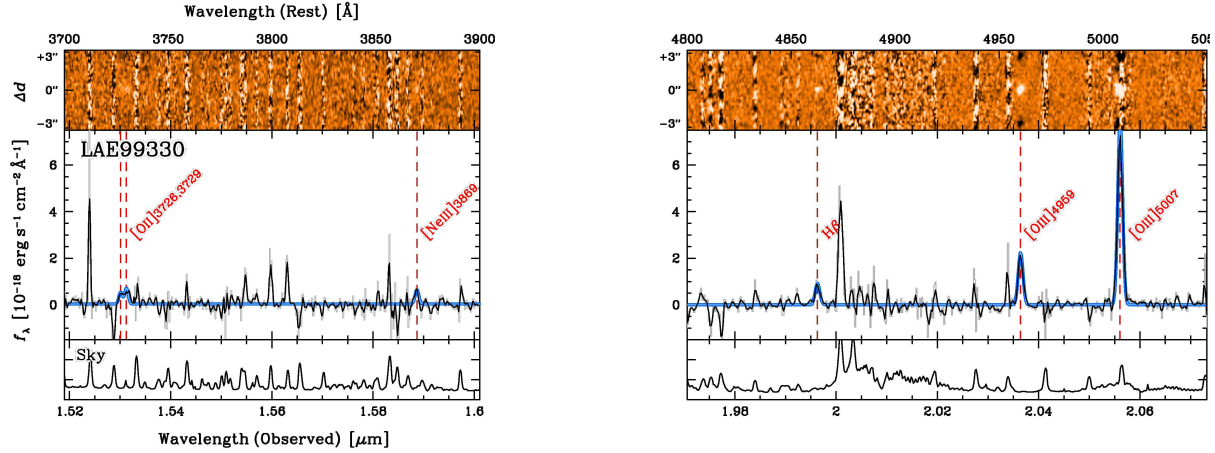


FIG. 2.— MOSFIRE H and K spectra of a representative $z = 3.105$ LAE. Detected emission lines are marked as vertical red-dashed lines, and the best-fit Gaussians are illustrated in blue.

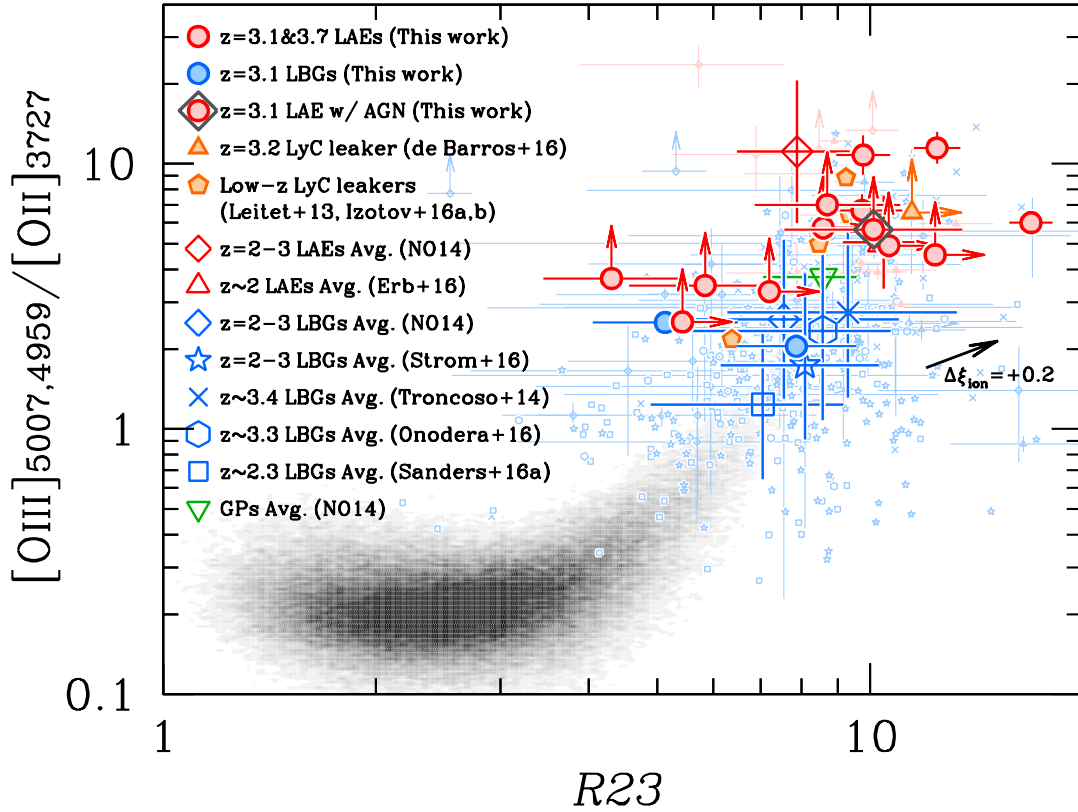


FIG. 3.— $[\text{O III}]\lambda\lambda 5007, 4959 / [\text{O II}]\lambda 3727$ line ratio versus $R23$ -index for the MOSFIRE and other samples. Red and blue filled circles represent the newly-observed LAEs and LBGs, respectively; the AGN86861 is shown with a grey-diamond. The orange triangle shows a LyC leaking candidate at $z = 3.2$ (*Ion2*, de Barros et al. 2016) and the orange pentagons are two nearby LyC leakers (Leitet et al. 2013) and five at $z \simeq 0.3$ (Izotov et al. 2016a,b) selected according to their high $[\text{O III}] / [\text{O II}]$ ratio. Other red and blue symbols are high- z LAEs and LBGs, respectively, compiled from the literature as shown in the legend. Grey shading illustrates the equivalent distribution for SDSS galaxies. The black arrow indicates the shift expected for a harder ionizing radiation (see text).

Figure 3 compares the results for our MOSFIRE $z \simeq 3.1$ sample with other high redshift and local sources in the $[\text{O III}] / [\text{O II}]$ ratio vs. the $R23$ -index plane. The latter index is a valuable probe of the gas-phase metallicity. For the newly-observed sample, we assume no dust correction, an assumption we return to in Section 3.3. In comparing with literature samples, we classify galaxies as LAEs if the rest $\text{EW}(\text{Ly}\alpha)$ exceeds 20 \AA (Nakajima & Ouchi 2014;

Erb et al. 2016), whereas for the UV-selected galaxies at $z = 2 - 4$ (Troncoso et al. 2014; Sanders et al. 2016a; Onodera et al. 2016; Strom et al. 2016), we assume these are dominated by LBGs (cf. Shapley et al. 2003). No obvious AGNs are included in the literature samples.

Since we are interested in the relevance of intense $[\text{O III}]$ emission as a possible indicator of a high f_{esc} we also plot recent galaxies revealing significant LyC emission; *Ion2* at $z = 3.2$ (de Barros et al. 2016; Vanzella et al. 2016), five green pea galaxies at $z \simeq 0.3$ (Izotov et al. 2016a,b),

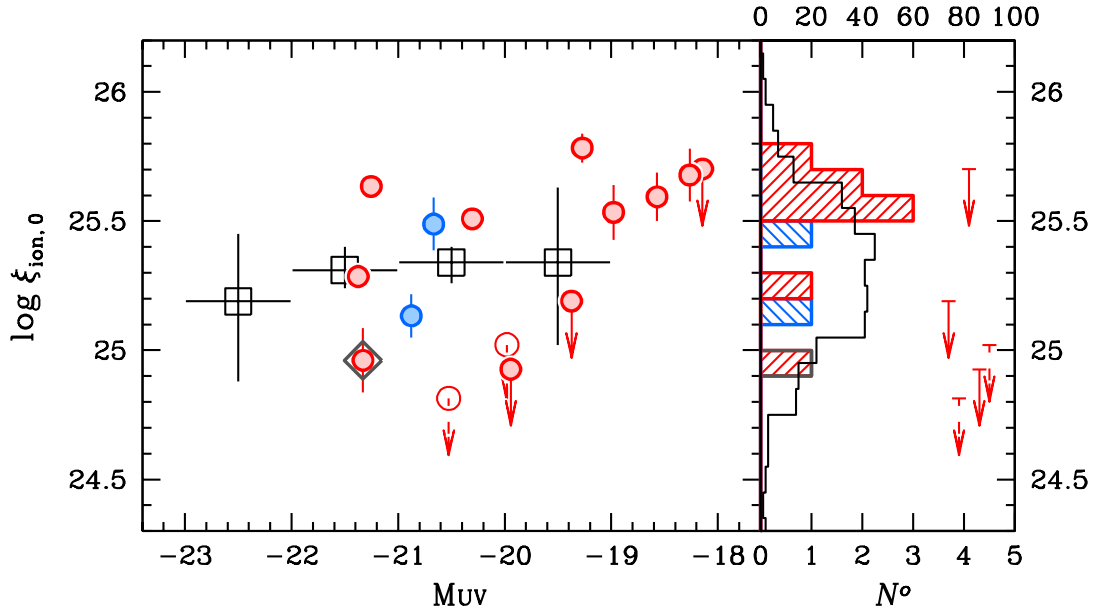


FIG. 4.— The ionization production parameter $\xi_{\text{ion},0}$ as a function of UV absolute magnitude (left) and its distribution (right; lower abscissa for our sample). Red and blue symbols refer to LAEs and LBGs respectively drawn from the current study. The grey-enclosed red symbol corresponds to AGN86861. Red down-pointing arrows indicate 3σ upper-limits for those sources for which $\text{H}\beta$ is not detected (open circles and dashed arrows show objects with less precise photometry). The black points and histogram (upper abscissa) indicates the $\xi_{\text{ion},0}$ for a larger sample of $z = 3.8 - 5.0$ LBGs for which $\text{H}\alpha$ was inferred from Spitzer photometry (Bouwens et al. 2015).

and two local galaxies (Bergvall et al. 2006; Leitet et al. 2013).

Firstly, following Nakajima & Ouchi (2014), it is clear that our LAEs have the highest $[\text{O III}]/[\text{O II}]$ ratio. A typical LBG at $z = 2-4$ has an $[\text{O III}]/[\text{O II}]$ ratio of $\sim 1-3$, whereas the LAEs presented here lie above $\simeq 3$ at the $> 3\sigma$ level with some as high as $\simeq 10$. Some LAEs may have even higher ratios given we cannot always detect $[\text{O II}]$. Notably, this LAE-LBG difference is seen even within our own sample.

Secondly, LAEs have an $[\text{O III}]/[\text{O II}]$ ratio higher than LBGs whose R23-indices are comparable. In local galaxies, a higher ionization parameter, q_{ion} , is found in less chemically-enriched galaxies. This correlation provides an empirical metallicity indicator for systems with strong line ratios (e.g., Maiolino et al. 2008). Although high- z LBGs appear to follow the same relation (e.g., Shapley et al. 2015; Sanders et al. 2016a,b), LAEs lie above this trend indicative of an enhanced ionization parameter (e.g., Nakajima & Ouchi 2014). LBGs have a metallicity of $\sim 0.2 - 0.3 Z_{\odot}$ at a R23-index $\simeq 10$ (Maiolino et al. 2008). On the other hand, if the $[\text{O III}]/[\text{O II}]$ ratio were adopted as a metallicity indicator (Maiolino et al. 2008), the LAEs would have metallicities lower than those based on the R23-index and the Kobulnicky & Kewley (2004) method by $0.4 - 1$ dex.

3.2. A Harder Ionizing Spectrum for LAEs

We now turn to estimating the ionizing photon production efficiency, ξ_{ion} , for our MOSFIRE sample using recombination lines in our spectra. This quantity represents the number of LyC photons per UV luminosity (Robertson et al. 2013; Bouwens et al. 2015);

$$\xi_{\text{ion}} = \frac{Q_{\text{H}\beta}}{L_{\text{UV}}} \quad (2)$$

where L_{UV} is the intrinsic UV-continuum luminosity. The LyC photons production rate is determined by massive young stars and best constrained by the hydrogen recombination lines, in this case $\text{H}\beta$: We adopt Bouwens et al. (2015) representation of the Leitherer & Heckman (1995) relation between $Q_{\text{H}\beta}$ and the $\text{H}\beta$ luminosity $L(\text{H}\beta)$, as

$$L(\text{H}\beta) [\text{erg s}^{-1}] = 1.36 \times 10^{-12} Q_{\text{H}\beta} / 2.86 [\text{s}^{-1}], \quad (3)$$

where a Case B recombination is adopted.

Note that the conversion assumes no escaping ionizing photons, i.e all are converted into recombination radiation. To recognize this, we adopt the notation $\xi_{\text{ion},0}$, whose zero subscript indicates that the escape fraction of ionizing photons is zero. The quantity ξ_{ion} can be derived by dividing $\xi_{\text{ion},0}$ by $(1 - f_{\text{esc}})$. The UV luminosity is measured from an SED around $1500 - 1600 \text{ \AA}$ using the appropriate rest-frame broadband photometry assuming zero reddening. The SED fitting was done as described in Kusakabe et al. (2015).

The assumption of zero reddening is important since it clearly affects ξ_{ion} . We note Schaerer et al. (2016) find dust correction decreases ξ_{ion} for LyC leakers at $z \simeq 0.3$ by $\sim 0.3 - 0.4$ dex. We return to this assumption in Section 3.3.

$\text{H}\beta$ is robustly detected in 10 of our 15 galaxies (7 LAEs, 2 LBGs and the AGN) and the derived values of $\xi_{\text{ion},0}$ are listed in Table 1. Figure 4 compares the distribution of $\xi_{\text{ion},0}$ as a function of the absolute UV magnitude for the various categories with those for $z = 3.8 - 5.0$ LBGs analysed using a similar approach based on inferred $\text{H}\alpha$ (Bouwens et al. 2015).

Again, the $\text{H}\beta$ -detected LAEs have an average $\xi_{\text{ion},0}$ larger than that inferred for $z = 3.8 - 5.0$ LBGs by $\sim 0.2 - 0.5$ dex. They support the contention deduced from Figure 3 that LAEs typically have a harder ioniz-

ing radiation field than LBGs. The difference is apparent at a fixed UV magnitude suggesting a higher production rate of ionizing photons.

The offset could be even larger if, as suspected from the large [O III]/[O II] ratio, f_{esc} is non-zero (see also Iwata et al. 2009; Nestor et al. 2013; Mostardi et al. 2013). For example, if $f_{\text{esc}} \simeq 0.3$, ξ_{ion} becomes larger than $\xi_{\text{ion},0}$ by ~ 0.15 dex. We note that two LAEs and one AGN-LAE have $\xi_{\text{ion},0}$ consistent with the LBG population. This might arise from a particularly high f_{esc} , a less significant Ly α emission ($\simeq 20\text{\AA}$), and/or a more mature stellar population (Robertson et al. 2013) inferred from SED fitting (> 500 Myr).

3.3. Constraints on Dust in LAEs

In the foregoing analyses, we have ignored any corrections for dust reddening in our sample which would otherwise affect the results we present in both Figures 3 and 4.

This assumption is supported by two LAEs in our sample, LAE93564 and LAE104037, for which we are fortunate to see multiple Balmer lines and where the Balmer decrements are consistent with zero reddening, albeit with an uncertainty of $\Delta E(B-V) = 0.1$. For the other LAEs, SEDs based on our multicolor Subaru photometry further restrict the range of $E(B-V)$ values consistent with zero to within 1σ . If we assume a median $E(B-V) = 0.03$ consistent with the SEDs and assume an SMC attenuation law¹⁴ (Gordon et al. 2003), and the same color excess for the stellar and nebular emission, $\xi_{\text{ion},0}$ is only decreased by ~ 0.1 dex. This would not change our conclusion that LAEs have a harder ionizing radiation field than LBGs. Of course, any residual correction for dust reddening effect has an even smaller effect on the [O III]/[O II] ratio (a decrease of ~ 0.02 dex) and the R23-index (an increase of < 0.01 dex).

4. DISCUSSION

We present Keck MOSFIRE measurements of the diagnostic nebular emission lines of [O III], [O II], and H β drawn from a sample of 15 $z \simeq 3.7$ and 3.1 LAEs and LBGs. In comparison with similar measurements of other surveys, we demonstrate that LAEs have much larger [O III]/[O II] line ratios than those seen in LBGs. This enhancement cannot be fully explained by their low metallicities, given the locally defined relation between metallicity and ionization parameter. There are three possible explanations for this difference - (i) a larger gas density, (ii) a higher production rate of ionizing photons (and thus a larger mean ξ_{ion}), and (iii) a different geometry of HII clouds (which relates to a higher f_{esc}). For (i)-(ii), following Equation (1), a dense ISM or a high production of ionizing photons will increase the [O III]/[O II] ratio.

We believe a denser ISM is an unlikely explanation because gas densities estimated from the resolved [O II] $\lambda 3729/\lambda 3726$ doublet line ratio for LAEs are, on average, comparable to typical values for $z \sim 2.3$ UV-selected LBGs ($\sim 200 \text{ cm}^{-3}$; Sanders et al. 2016a). Although only two of our LAEs have a well-measured [O II]

doublet ratio, both indicate a modest gas density of $50\text{--}300 \text{ cm}^{-3}$.

A higher production rate of ionizing photons is a more natural explanation for the high [O III]/[O II] ratio as we have directly verified they have a high $\xi_{\text{ion},0}$. However, the $0.3\text{--}0.5$ dex larger $Q_{\text{H}\alpha}$ observed would only increase the ionization parameter q_{ion} by $0.1\text{--}0.17$ dex and the [O III]/[O II] ratio by $\sim 0.12\text{--}0.2$ dex at a fixed metallicity of $\sim 0.2\text{--}0.3 Z_{\odot}$ (i.e., $R23 \sim 10$; Kobulnicky & Kewley 2004).

Additionally, the ionizing spectrum may be harder. In this case we also expect an enhancement in the R23-index. We can calculate the magnitude of this effect using photoionization models similar to those presented in Nakajima & Ouchi (2014), varying the stellar metallicity to represent a change in the hardness of the radiation field. We assume a gas phase metallicity of $Z \sim 0.5 Z_{\odot}$ and an ionization parameter of $\log q_{\text{ion}} \sim 7.75$ (Sanders et al. 2016a; Onodera et al. 2016). To simulate the effect of a harder spectrum, we compare two stellar metallicity cases: $0.5 Z_{\odot}$ comparable to the gas-phase metallicity (e.g., Kewley et al. 2013) and a low value of $0.01 Z_{\odot}$. With these assumptions, our photoionization models predict both the [O III]/[O II] ratio and R23-index increase in the low metallicity case by only 0.1 dex, with ξ_{ion} enhanced by 0.2 dex. This change is illustrated in Figure 3 with a black arrow. This change of ξ_{ion} originates from the reduced UV-continuum since we fix the ionization parameter. If, conversely, the UV-continuum level is fixed, the higher ξ_{ion} would further increase the ionization parameter by ~ 0.06 dex and [O III]/[O II] ratio only by ~ 0.08 dex. Neither is sufficient to explain the high [O III]/[O II] ratio.

The third explanation would indicate a strong connection between the large [O III]/[O II] ratio and the escape fraction f_{esc} (Nakajima & Ouchi 2014). If HII regions are density-bound, the nebulae have a low column density of HI and a high f_{esc} . The large [O III]/[O II] ratio arises since the outer zone that produces [O II] is reduced while the inner [O III]-producing zone is unchanged (e.g., Kewley et al. 2013). The R23-index is largely unaffected since hydrogen will be ionized throughout the nebula. For the ISM properties of a LBG, our photoionization models predict an [O III]/[O II] ratio enhanced by 0.4 dex with an unchanged R23-index (0.02 dex decrease) for f_{esc} of 30 %. This explanation is compatible with the modest densities observed in the LAEs, since the [O II] doublet probes the ionized gas density while density-bound nebulae only affect the HI density.

The only way to test whether such density-bounded HII regions are dominant in high- z LAEs and that this provides a contribution to the large [O III]/[O II] ratios, is to directly constrain the LyC leakage from $z \simeq 3$ LAEs. This would permit us to break the degeneracies in the discussion above. The prospects appear promising given the similarity in line emission properties with the sources recently observed successfully with LyC photons (Vanzella et al. 2016; Izotov et al. 2016a,b; Schaerer et al. 2016). Regardless of the above degeneracy, our sample of $z \simeq 3$ LAEs represent valuable low redshift analogs of the $z > 7$ sources with similarly intense [O III] emission and harder ionizing spectra (Stark et al. 2015a,b; Sobral et al. 2015; Stark et al. 2016) that may

¹⁴ As adopted in Figure 4 for Bouwens et al. (2015)'s $\xi_{\text{ion},0}$ measurements.

have the necessary high f_{esc} to drive cosmic reionization.

We are grateful to the staff of the W. M. Keck Observatory who keep the instrument and telescope running effectively. We thank Dan Stark for encouragement and useful comments. We also thank T. Hayashino, T. Yamada, and Y. Matsuda for providing the LAE catalog and some of the photometric and spectroscopic data,

and R. Bouwens for providing $\xi_{\text{ion},0}$ measurements of $z = 3.8 - 5.0$ LBGs.

KN acknowledges the JSPS Postdoctoral Fellowships for Research Abroad, and was benefited from a MERAC Funding and Travel Award for this project. RSE acknowledges support from the European Research Council through an Advanced Grant FP7/669253.

Facilities: Keck I (MOSFIRE)

REFERENCES

- Bergvall, N., et al. 2006, *A&A*, 448, 513
 Bouwens, R. J. et al. 2015, arXiv-eprints, arXiv:1511.08504
 de Barros, S., et al. 2016, *A&A*, 585, A51
 Erb, D. K., et al. 2016, arXiv-eprints, arXiv:1605.04919
 Fan, X., et al. 2004, *ApJ*, 128, 515
 Gordon, K. D., et al. 2003, *ApJ*, 594, 279
 Hayashino, T., et al. 2004, *AJ*, 128, 2073
 Iwata, I., et al. 2009, *ApJ*, 692, 1287
 Izotov, Y. I., et al. 2016a, *Nature*, 529, 178
 Izotov, Y. I., et al. 2016b, *MNRAS*, 461, 3683
 Kewley, L. J., et al. 2013, *ApJ*, 774, 100
 Kobulnicky, H. A., Kewley, L. J. 2004, *ApJ*, 617, 240
 Kusakabe, H., Shimasaku, K., Nakajima, K., & Ouchi, M. 2015, *ApJ*, 800, L29
 Leitert, E., Bergvall, Hayes, M., Linné, S., & Zackrisson, E. 2013, *A&A*, 553, A106
 Leitherer, C., & Heckman, T. M. 1995, *ApJS*, 96, 9
 Maiolino, R., et al. 2008, *A&A*, 488, 463
 Malhotra, S. et al. 2012, *ApJ*, 750, L36
 Micheva, G., et al. 2015, arXiv-eprints, arXiv:1509.03996
 Micheva, G., et al. 2016, arXiv-eprints, arXiv:1604.00102
 Mostardi, R. E., et al. 2013, *ApJ*, 779, 65
 Nakajima, K., & Ouchi, M. 2014, *MNRAS*, 442, 900
 Nestor, D. B., et al. 2013, *ApJ*, 765, 47
 Onodera, M. et al. 2016, *ApJ*, 822, 42
 Robert-Borsani, G. W., et al. 2015, arXiv-eprints, arXiv:1506.00854
 Robertson, B., et al. 2013, *ApJ*, 768, 71
 Robertson, B., Ellis, R. S., Furlanetto, S. R., & Dunlop, J. S. 2015, *ApJ*, 802, L19
 Sanders, R. L., et al. 2016a, *ApJ*, 816, 23
 Sanders, R. L., et al. 2016b, arXiv-eprints, arXiv:1606.00053
 Schaerer, D., et al. 2016, arXiv-eprints, arXiv:1606.00053
 Schenker, M. A., Ellis, R. S., Konidakis, N. P., & Stark, D. P. 2013, *ApJ*, 777, 67
 Shapley, A. E., et al. 2003, *ApJ*, 588, 65
 Shapley, A. E., et al. 2015, *ApJ*, 801, 88
 Smit, R., et al. 2014, *ApJ*, 784, 58
 Smit, R., et al. 2015, *ApJ*, 801, 122
 Sobral, D., et al. 2015, *ApJ*, 808, 139
 Stark, D. P., et al. 2015a, *MNRAS*, 450, 1846
 Stark, D. P., et al. 2015b, *MNRAS*, 454, 1393
 Stark, D. P., et al. 2016, arXiv-eprints, arXiv:1606.01304
 Steidel, C. C., et al. 2014, *ApJ*, 795, 165
 Strom, A. L., et al. 2016, arXiv-eprints, arXiv:1608.02587
 Troncoso, P., et al. 2014, *A&A*, 563, A58
 Vanzella, E., et al. 2016, arXiv-eprints, arXiv:1602.00688
 Yamada, T., et al. 2012, *ApJ*, 143, 79
 Zitrin, A., et al. 2015, *ApJ*, 810, L12

TABLE 1
SPECTRAL AND STELLAR PROPERTIES OF THE MOSFIRE-IDENTIFIED LAEs AND LBGs

Obj.	EW(Ly α) (\AA) (1)	spec(FUV)? (2)	z_{nebular} (3)	[O III]/[O II] (4)	R23 (5)	$\log \xi_{\text{ion},0}$ (Hz erg $^{-1}$) (6)	$\log \text{SFR}_0$ ($M_{\odot} \text{yr}^{-1}$) (7)	$\log M_{\star}$ (M_{\odot}) (8)	M_{UV} (AB) (9)
LAE93564	61^{+4}_{-4}	yes	3.6768	10.78 ± 2.0	9.8 ± 0.9	25.63 ± 0.04	1.80 ± 0.04	$10.28^{+0.27}_{-1.21}$	-21.3
LAE94460(†)	54^{+9}_{-8}	yes	3.0721	> 2.5	> 5.4	< 25.0	< 0.68	$9.10^{+0.39}_{-0.73}$	-20.0
LAE97081	> 213	yes	3.0760	> 4.9	> 10.6	< 25.70	< 0.63	$8.08^{+0.70}_{-0.72}$	-18.1
LAE97176	62^{+15}_{-13}	yes	3.0749	> 4.5	> 12.4	< 24.93	< 0.57	$9.28^{+0.31}_{-0.71}$	-19.9
LAE103371	151^{+72}_{-47}	yes	3.0892	> 7.0	8.7 ± 2.3	25.68 ± 0.10	0.65 ± 0.10	$9.87^{+0.26}_{-0.72}$	-18.3
LAE104037	37^{+3}_{-3}	yes	3.0646	6.0 ± 0.3	16.9 ± 1.2	25.29 ± 0.03	1.51 ± 0.03	$9.95^{+0.09}_{-0.13}$	-21.4
LAE89723(†)	43^{+7}_{-7}	no	3.1109	> 3.3	> 7.2	< 24.81	< 0.69	$8.47^{+1.06}_{-0.39}$	-20.5
LAE91055	> 77	no	3.0814	> 3.7	4.3 ± 1.1	25.59 ± 0.09	0.69 ± 0.09	$8.80^{+0.82}_{-1.36}$	-18.6
LAE97030	26^{+11}_{-9}	no	3.0731	6.7 ± 1.0	9.7 ± 1.4	25.78 ± 0.06	1.16 ± 0.06	$8.41^{+0.68}_{-0.57}$	-19.3
LAE97254	74^{+27}_{-20}	no	3.0709	> 3.5	5.8 ± 1.6	25.53 ± 0.11	0.79 ± 0.11	$9.14^{+0.56}_{-0.41}$	-19.0
LAE99330	48^{+7}_{-6}	no	3.1054	11.5 ± 1.7	12.4 ± 1.0	25.51 ± 0.03	1.30 ± 0.03	$10.64^{+0.33}_{-0.67}$	-20.3
LAE104147	24^{+7}_{-6}	no	3.0991	> 5.7	> 8.6	< 25.19	< 0.61	$9.37^{+0.41}_{-0.83}$	-19.4
AGN86861	79^{+3}_{-3}	yes	3.1051	> 5.6	10.1 ± 3.4	24.96 ± 0.12	1.16 ± 0.13	$10.52^{+0.03}_{-0.04}$	-21.3
LBG102826	-4^{+4}_{-3}	yes	3.0710	2.0 ± 0.2	7.9 ± 1.7	25.13 ± 0.08	1.15 ± 0.08	$9.80^{+0.08}_{-0.23}$	-20.9
LBG104097	-1^{+8}_{-6}	yes	3.0671	2.5 ± 0.2	5.1 ± 1.4	25.49 ± 0.10	1.42 ± 0.10	$9.69^{+0.18}_{-0.16}$	-20.7

NOTE. — Column (1) shows the rest EW(Ly α). For the $z \simeq 3.1$ objects, the EW is estimated from the BV–NB497 color. The EW of the $z = 3.7$ LAE is derived based on the spectroscopic measurement of the Ly α flux and the V-band photometry. A 3σ lower-limit is given if the object is not detected significantly in the BV image. Column (2) illustrates if the object had a previous spectroscopic confirmation in the FUV. Column (3) presents the nebular redshift. Columns (4) and (5) give the [O III] $\lambda\lambda 5007, 4959$ /[O II] $\lambda 3727$ ratio and the R23-index, respectively. Column (6) presents ξ_{ion} under the assumption of a zero f_{esc} . Column (7) shows the SFR under the assumption of a zero f_{esc} , estimated from the H β luminosity. An upper-limit of 3σ is adopted in Columns (4)–(7) if the line is not detected. Column (8) gives the stellar mass derived from SED fitting, which adopts an SMC dust law. Column (9) is the absolute UV magnitude measured from an SED around 1500 – 1600 \AA . (†) The $\xi_{\text{ion},0}$, stellar mass, and M_{UV} estimates are less certain due to less precise optical photometry.